



Nanocrystalline ZnO doped Dy₂O₃ a highly active visible photocatalyst: The role of characteristic f orbital's of lanthanides for visible photoactivity

G.A. Suganya Josephine, A. Sivasamy*

Chemical Engineering Area, CSIR-Central Leather Research Institute, Adyar, Chennai 600020, India



ARTICLE INFO

Article history:

Received 1 August 2013

Received in revised form 28 October 2013

Accepted 4 November 2013

Available online 12 November 2013

Keywords:

Nanocrystalline

Photocatalyst

ZnO

Dy₂O₃

Degradation

ABSTRACT

Nanocrystalline ZnO doped Dy₂O₃ has been prepared by a simple and efficient technique for exhibiting an enhanced visible light photocatalytic activity. The prepared catalysts were characterized by IR, UV-DRS, XRD, FESEM, EDAX, HRTEM, XPS, AFM and EPR analysis. XRD data showed that the particles were highly crystalline and nanosized. The size of the nanoparticle was 30–56 nm and found to be of mixed morphology. The surface of the catalyst was highly porous and had a surface roughness of 53.28 nm. ZnO was doped on Dy₂O₃ in various proportions and the best ratio was finalized by the determination of photodegradation efficiency employing a model pollutant for example, ORG under visible light irradiation. 50 mol% ZnO doped Dy₂O₃ possessed two fold photocatalytic activities than that of pristine ZnO and followed a pseudo-first-order degradation kinetics. The enhanced photocatalytic activity was due to the presence of f shells in the lanthanide oxide crystal lattice which traps the excited electrons further delaying the process of recombination of electron-hole pair. The dye degradation was initiated by the attack of OH radicals formed during the course of reaction and the formation of OH radicals was confirmed by EPR analysis. The 50 mol% ZnO doped Dy₂O₃ catalyst completely degraded ORG dye molecules in the aqueous phase and these were confirmed by UV-visible spectroscopy, COD and QTOF-Mass analyses.

© 2013 Elsevier B.V. All rights reserved.

1. Introduction

Photocatalysis has been investigated as a very efficient technique for various light induced processes such as mineralization of toxic organic, inorganic and biological materials [1–3], electrochemical splitting of water [4], etc. Effluents from industrial wastewater and discharges from tannery and textile industries mainly contains dyes and pigments which are a serious hazard to the environment and human health as they are carcinogenic and non-biodegradable [5]. Extensive studies on photodegradation of organic dyes employing metal oxides and modified metal oxides semiconductors have been carried out by various research groups. Due to stringent environmental regulations, toxic organics and inorganics have to be removed before they are released into the aquatic environment. Therefore, there is a need to develop less energy intensive and effective new photocatalytic system for purification of organics loaded water and wastewater using renewable energy source like solar energy.

Photocatalysis generally employ UV, visible and solar light irradiations in particular visible light induced photocatalysis has received much attention due to its energy efficiency, as the solar energy spectrum consists of only 5–7% of UV light when compared to a higher fraction of 46% visible and 47% infrared radiations [6]. A catalyst which lies within the band gap of a semiconductor, possessing the required redox potential for the formation of hydroxyl radicals (OH•), super oxide (O₂•⁻), etc., from water [7] is considered to be very effective. Heterogeneous metal oxide semiconductor photocatalysis has received much attention in recent past employing TiO₂ and ZnO, as it has a required band gap of 3.2 eV [8–17]. ZnO and ZnO based photocatalysts are preferred over TiO₂ due to their high quantum efficiency [18]. Efforts have been taken to enhance the activity of the metal oxides in the visible region by creation of oxygen vacancies [19–21], semiconductor coupling [22], surface modification by incorporation of organic materials [23,24], metal and non-metal doping [25–33]. Rare earth doped TiO₂ have been exploited recently for the degradation of organic compounds [34–36] and only few reports are available for rare earth metal ion doped ZnO [37,38] and its visible photocatalytic activity. Lanthanides are a group of elements generally used in various fields for its optical characteristics and its luminescence emission capabilities. Nowadays lanthanides play a major role in preparing light emitting diodes, optical fibers, amplifiers and biomedicine. For

* Corresponding author. Tel.: +91 044 24912150; fax: +91 044 24911589.

E-mail addresses: arumugamsivasamy@yahoo.co.in, sivasamy.arumugam@gmail.com (A. Sivasamy).

example Tb^{3+} , Eu^{3+} and Dy^{3+} are used for emission of green, red and white light respectively [39–41]. Since it possesses optical characteristics and photoluminescence, this property can be utilized for the preparation of photocatalyst by doping rare earth's onto oxides like ZnO , TiO_2 , etc. Various metal oxides and insulators have already been used as a base material for the enhancement of surface area to develop better hybrid catalytic systems but the band gap alterations of these materials have not been reported [42]. Oxides of lanthanide generally possess large band gaps and are listed under the category of insulators [43]. Dy_2O_3 (band gap 4.8 eV) [44] has been doped on ZnO and studied for various applications other than photocatalysis induced by visible light irradiation [45–55], particularly for its optical and luminescent activity. Therefore, studies employing the doping of a commercially available metal oxide like ZnO onto the rare earth element possessing a very high band gap would be a new approach, also f – f transitions which are characteristic of lanthanide elements would be a support to enhance its visible photocatalytic activity. Where, the f shells of lanthanide elements trap the electrons during the process of visible light irradiation as reported elsewhere on rare earth doped TiO_2 [56–61]. Therefore, tuning of band gap energy in lanthanide insulators by doping of semiconductors is a novel approach to enhance the visible light absorption which may lead to enhanced visible light photocatalysis and it may find varied applications in environmental remedial purposes.

We report herein a process for the transformation of an insulator like Dy_2O_3 into a visible light active photocatalyst, by the process of doping ZnO onto Dy_2O_3 . To the best of our knowledge this is the first report employing a rare earth oxide with higher energy band gap as one of the major oxides for photocatalytic application. Nanocrystalline (NC) ZnO doped Dy_2O_3 have been synthesized and characterized by FT-IR, UV-DRS, XRD, FESEM, EDAX, HRTEM, XPS, AFM and EPR techniques. The photocatalytic activities of the prepared catalyst have been carried out for the degradation of a model pollutant such as ORG.

2. Experimental

2.1. Chemicals

Zinc nitrate hexahydrate (98%, $\text{Zn}(\text{NO}_3)_2 \cdot 6\text{H}_2\text{O}$) and Dysprosium Nitrate (99.9%, $\text{Dy}(\text{NO}_3)_3 \cdot 6\text{H}_2\text{O}$) were purchased from Sigma–Aldrich, India. Orange G dye (90%, 7-hydroxy-8-phenylazo-1,3-naphthalenedisulfonic acid disodium salt) and Na_2CO_3 supplied by S.D. Fine Chem., Mumbai, India. DMPO (5,5-dimethyl-1-pyrroline-N-oxide) purchased from Sigma–Aldrich, India. All the chemicals except DMPO were used as such without further purification. DMPO was purified and checked for purity before analysis.

2.2. Preparation of the Photocatalyst

ZnO doped Dy_2O_3 was prepared by a modified method [52] reported elsewhere. A typical procedure as follows: aqueous solutions of precursors $\text{Dy}(\text{NO}_3)_3 \cdot 6\text{H}_2\text{O}$, $\text{Zn}(\text{NO}_3)_2 \cdot 6\text{H}_2\text{O}$ and Na_2CO_3 were prepared in double-distilled water to obtain the required stoichiometry. The zinc, dysprosium oxide precursors and carbonate were taken in a 1:1 ratio. In a vigorously stirred solution of 10 ml 0.1 M dysprosium nitrate, 10 ml of 0.1 M Na_2CO_3 was slowly added until the formation of white suspension. Then 10 ml of 0.1 M zinc nitrate was added slowly into the suspension with continuous stirring followed by slow addition of 10 ml 0.1 M Na_2CO_3 . The mixture was stirred continuously for another 30 min and filtered. The precipitate was washed thoroughly with water and finally with ethanol for the removal of residual carbonates. The white

precipitate was collected, dried at 100 °C for 12 h and sintered at 700 °C for 2 h in a tubular furnace. Pristine dysprosium oxide, zinc oxide and doping were carried out by a similar method employing the required stoichiometry of the reactants. The doping concentrations of ZnO on Dy_2O_3 are represented as 0, 10, 20, 30, 50 and 100 mol% namely ZnO , ZnDy 10:90, ZnDy 20:80, ZnDy 30:70, ZnDy 50:50, Dy_2O_3 .

2.3. Instrumental analysis

The prepared photocatalysts were characterized by FT-IR, XRD, UV-DRS, FESEM, HRTEM, XPS, AFM and EPR techniques. The metal oxide stretching frequencies were determined by FT-IR measurement (Perkin Elmer FT-IR spectrometer). The crystallinity of the prepared photocatalyst was characterized by XRD (PAN analytical X-ray diffractometer, Germany) with $\text{Cu K}\alpha$ radiation in the 2θ scan range between 10° and 70°. An accelerating voltage of 40 kV and an emission current of 25 mA were used. The surface morphology, size of particle and doping percentage of the sample were analyzed by FESEM and EDAX (Model Supra 55 – Carl Zeiss, Germany). The surface roughness and porosity of the sample were determined by atomic force microscopy technique (Model-NTEGRA PRIMA-NTMDT, Ireland) by using the contact mode. The UV-DRS of the sample was determined by UV 2600, Shimadzu, Japan using a scan speed of 200 nm/min. The photocatalytic degradation of the dye molecules were monitored by UV–visible spectrophotometer (Shimadzu UV-2101PC, Japan). COD analyses of the samples were carried out in a Thermo reactor (HACH DRB 200). The HRTEM analysis was carried out in a JEOL 3010 instrument. X-ray photoelectron spectroscopy (XPS) measurements were conducted using an Omicron ESCA Probe spectrometer. In situ generations of OH radicals were analyzed by the EPR technique using Bruker model EMX X Band, electron paramagnetic resonance spectrometer. Mass spectral analyses were carried out in a quadrupole-time of flight mass spectrometer with mass lynx data processor.

2.4. Photocatalytic studies

The photocatalytic studies were performed in an annular Type Photo reactor (Heber Scientific Company Ltd., Chennai, India). A 500 W tungsten halogen lamp was used as the irradiation source. The photocatalytic reactor tubes were made of glass with 30 cm × 1.5 cm (height × diameter) and 30 cm × 3.5 cm. The visible light emitting lamp was surrounded with a water jacketed tube which was continuously cooled with water circulation to remove the heat produced by the lamp. For the preliminary photocatalytic experiments, 10 ml of the required concentration of dye solution made up in the required pH and appropriate amount of catalyst, were taken in the reaction tubes of the photo reactor and subjected to visible light irradiation with continuous stirring. The kinetics of visible light induced photocatalytic degradation of Orange G (ORG) dye, (Fig. S1, Supplemental Information) were studied with a volume of 150 ml of dye solution and required amount of catalyst. Aliquots of the sample were withdrawn at regular time intervals and their absorbances were measured. The residual concentration of the targeted compound before and after photocatalytic degradation has been computed from the calibration chart and hence the percentage degradation of the dye molecule was calculated using Eq. (1).

$$\text{Degradation efficiency(\%)} = \frac{C_0 - C_e}{C_0} \times 100 \quad (1)$$

where, C_0 and C_e are the initial and final dye concentrations in the aqueous phase respectively.

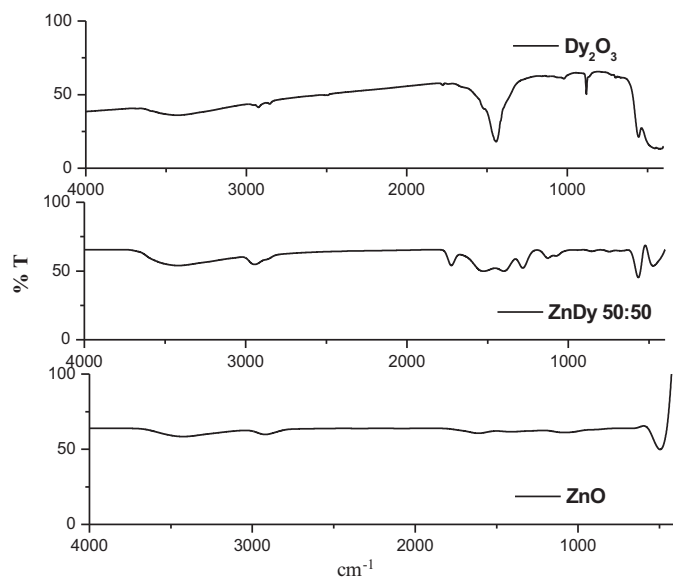


Fig. 1. Infra red spectrums of ZnO, ZnDy 50:50 and Dy₂O₃ photocatalysts.

3. Results and discussion

3.1. Characterization by Fourier transformed-infra red spectroscopy

The FT-IR spectrum of the prepared catalyst is shown in Fig. 1. The presence of Zn–O stretching vibrations at 490.32 cm^{−1} for ZnO and Dy–O stretching vibrations at 557.52 and 472.2 cm^{−1} for Dy₂O₃ were shown in figure and these results are compared with literature [62,63] data. The FT-IR spectra of ZnDy 50:50 photocatalyst showed only two peaks at 559.14 and 460.22 cm^{−1} and not three, because the peak arising from Zn–O and Dy–O are in the same wavelength region near 430–480 cm^{−1}. These results indicate that both zinc and dysprosium are present as oxides in the catalyst. In addition to these, few peaks are observed at 1200–1800 cm^{−1} which is probably due to the absorption of CO₂ by the catalyst and a peak at 3350 cm^{−1} is due to the presence of moisture in the sample.

3.2. Characterization of the photocatalyst by X-ray diffraction technique

The XRD patterns of pristine ZnO, Dy₂O₃ and ZnDy 50:50 are represented in Fig. 2. The diffraction peaks of pristine ZnO and Dy₂O₃ are similar to the standard patterns (ZnO–JCPDS No. 36–1451 and Dy₂O₃ – JCPDS 01-079-1722) [52]. It was observed that peaks in the XRD pattern at (2 1 1), (2 2 2), (4 0 0), (4 4 0) and (6 2 2) are characteristic planes for pristine Dy₂O₃ and at (1 0 0), (0 0 2), (1 0 1), (1 0 2), (1 1 0), (1 0 3), (0 0 4), (1 1 2) and (2 0 1) are characteristic planes for pristine ZnO. As the doping concentration of ZnO on Dy₂O₃ increases we could clearly observe the following: The diffraction due to the plane (2 2 2) is the major peak for all the samples containing Dy₂O₃. As the doping concentration of ZnO increases from 10 to 50% with respect to Dy₂O₃ it was observed that major characteristic planes of ZnO such as (1 0 0), (0 0 2), (1 0 1) starts to appear in the XRD pattern of the prepared catalysts.

For ZnDy 10:90 sample, only peaks due to Dy₂O₃ are present which shows that Zn²⁺ has been substituted for Dy³⁺ in the crystal lattice, since the atomic radii of Dy³⁺ (0.091 nm) is comparable with Zn²⁺ (0.083 nm), two Dy³⁺ ions could have been replaced by three Zn²⁺ ions thus creating Dy³⁺ ion vacancies. These results were

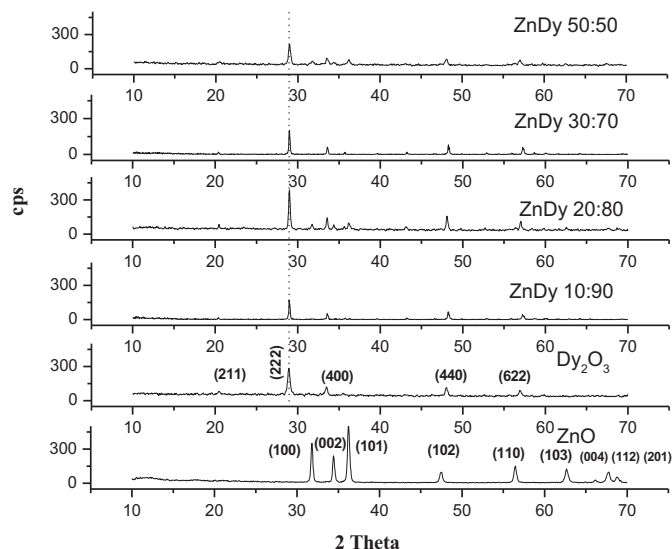


Fig. 2. X-ray diffraction patterns of (i) Dy₂O₃ neat (ii) ZnO neat (iii) and ZnDy 50:50.

corroborated with published literature data [64,65]. As shown in Table 1, there is a remarkable change in the lattice constant “a” which may be due to the increase of ZnO doping onto Dy₂O₃ and also a shift in the 2 theta values which correspond to the substitution of Dy³⁺ by Zn²⁺ in the catalyst matrix. In addition to this crystallite size also been calculated and given in Table 1. The peaks are higher and narrower indicating that the sample is in a highly ordered and crystalline state. The average size of the crystallite were found to be in the nano range of 34–51 nm calculated using the Scherer equation (2),

$$D = \frac{k\lambda}{B \cos \theta} \quad (2)$$

where, k is taken as 0.94 for spherical samples, λ the wavelength of radiation corresponding to 0.154 nm and B is the full width at half maximum and θ half the diffraction angle. From the published reports we come to know that even for lesser amount of dopant concentration (less than 0.5 at%) phases of the dopant were present in the XRD data [49,66,67], these reports explain that on increase in the dopant concentrations few atoms were substituted or present in the interstitial sites of the crystal lattice and the remaining were present as clusters which gave rise to diffraction peaks of the dopant in the spectrum. In addition while examining the phases of ZnO in the doped samples, it was observed that phases due to (1 0 0), (0 0 2) and (1 0 1) were visible and the other phases were negligible for doping concentrations more than 20 percent.

3.3. Surface morphology by field emission scanning electron microscopy and energy dispersive X-ray diffraction

The field emission-scanning electron microscopy images of pristine ZnO, Dy₂O₃ and ZnDy 50:50 are shown in Fig. 3 respectively. The particle sizes were calculated from FESEM images and they were in the nano range from 40 to 70 nm for all the three samples. The surface morphology of ZnO is nearly spherical and that of Dy₂O₃ is irregular. In ZnDy 50:50 catalyst it is observed that there are two morphologies existing, i.e., ZnO is uniformly coated on Dy₂O₃. The percentage of ZnO doping onto Dy₂O₃ was confirmed by EDAX analysis which shows that nearly 50 mol% of Zn and Dy are present in the catalyst.

Table 1

Displays the lattice parameters of the prepared photocatalysts.

S. No.	Photocatalyst composition	2 Theta	Lattice parameter 'a' (nm)	Cell volume (nm)	Crystallite size (nm)
1.	Dy ₂ O ₃	28.9228	1.0687	1.2207	34.172
2.	ZnDy 10:90	28.998	1.0660	1.2114	46.605
3.	ZnDy 20:80	28.9917	1.0661	1.2118	51.265
4.	ZnDy 30:70	28.9973	1.0663	1.2123	43.934
5.	ZnDy 50:50	28.9721	1.0669	1.2144	34.175

3.4. High-resolution transmission electron microscopy and X-ray photoelectron spectroscopy

The prepared photocatalyst ZnDy 50:50 has been analyzed by HRTEM technique. It was observed that the bright field HR-TEM image of the doped photocatalyst clearly showed that ZnO was completely doped on Dy₂O₃ phase and the crystalline arrangement of both the atoms were also observed in the selected area electron diffraction (SAED) pattern in the inset of Fig. 4 of the prepared ZnDy 50:50 photocatalyst. The particle size of the prepared catalyst ranged from 30 to 56 nm and it was observed that both zinc and dysprosium ions were present as oxides in the prepared sample as shown in the EDAX elemental analysis (Fig. 4). Further, to support the doping mechanism of the prepared photocatalyst (ZnDy 50:50), the samples were also analyzed by X-ray photoelectron spectroscopy and the results were provided in Supplementary Information (Fig. S2). It shows the Dy 4d, O 1s and Zn 2p spectrum of

the 50 mol% ZnO doped Dy₂O₃ photocatalyst. The spectrum clearly shows a line at 155.95 corresponding to Dy orbital of 4d_{5/2}. The O 1s spectrum showed a sharp peak centered at 531.23 which is mainly assigned to Dy–O oxygen bond, together with this an additional shoulder at 530.73 is observed which is attributed to Dy–O–Dy bond, and Dy–O–Zn bond respectively. Peaks at 1021.21 and 1044.38 correspond to Zn orbital of 2p_{3/2} and Zn 2p_{1/2} respectively. These results serve as a support for the doping of ZnO onto Dy₂O₃.

3.5. Surface morphology by atomic force microscopy

The AFM images of the ZnDy 50:50 photocatalysts were shown in Fig. 5 and it clearly indicates the surface roughness and porosity of the catalyst. The average surface roughness was found as 53.28 nm. The observation from AFM analyses confirms that the particles are nanosized. High surface roughness and lower size of the particle reveals that the surface is highly porous in nature. Hence,

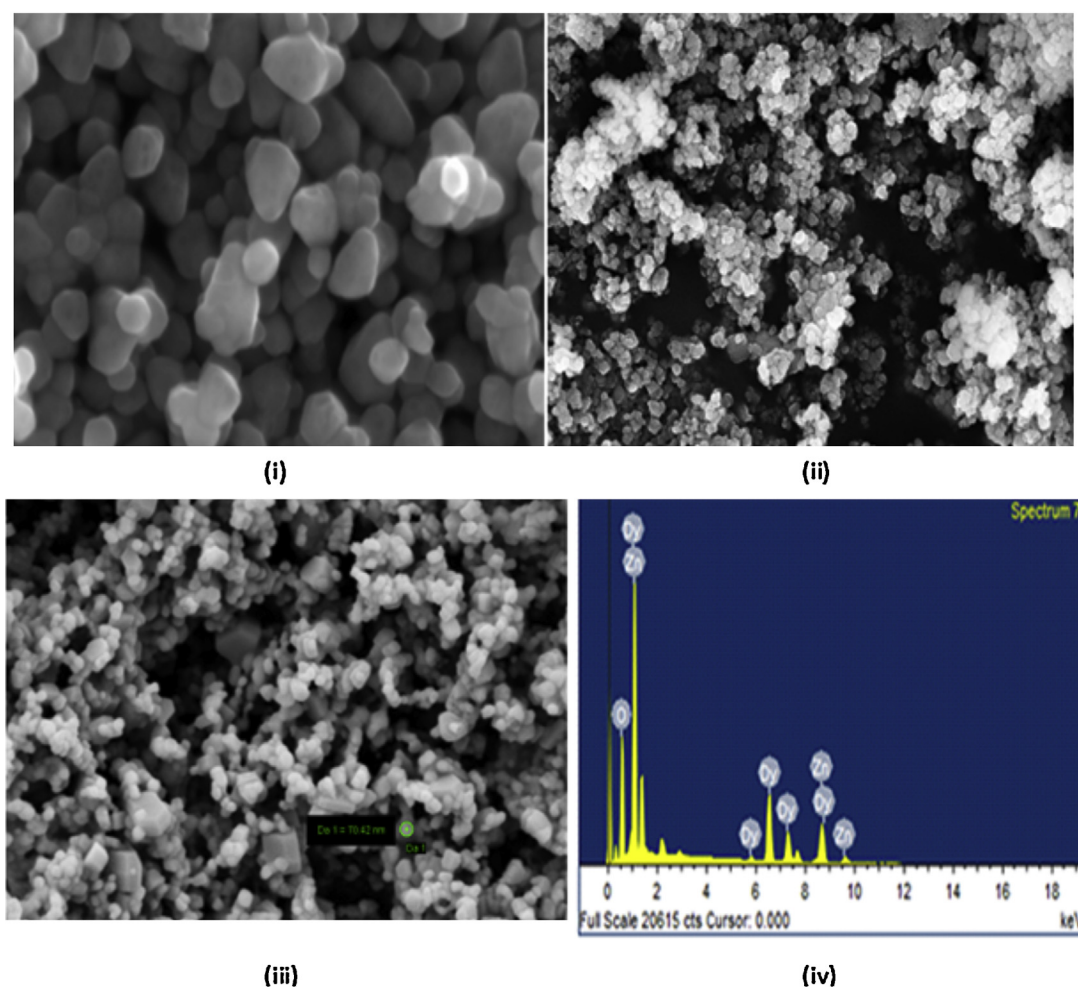


Fig. 3. Field emission-scanning electron microscopy images of (i) ZnO (ii) Dy₂O₃ (iii) ZnDy 50:50 catalysts and (iv) the energy dispersive X-ray spectroscopy image of ZnDy 50:50 showing 50% Zn doped Dy₂O₃.

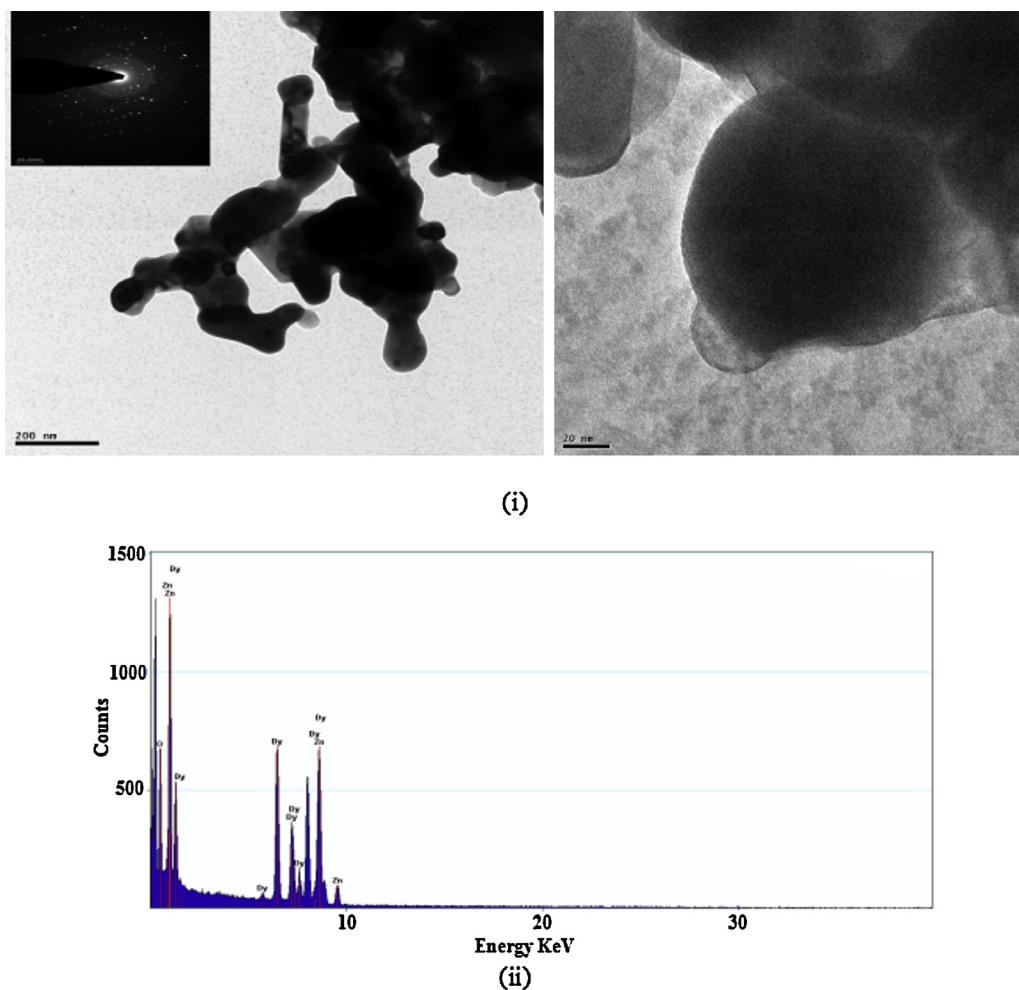


Fig. 4. (i) HRTEM images and (ii) EDAX spectrum of the prepared photocatalyst ZnDy 50:50.

the catalyst has a high surface area which is responsible for the enhanced photocatalytic activity of the photocatalyst. The surface roughness profile of the photocatalyst is also shown in Fig. 5(iv). The surface porosity and roughness in the photocatalysts permits the adsorption of dye molecules onto the surface, thereby increasing the rate of photodegradation.

3.6. Characterization by UV–visible diffuse reflectance spectroscopy

The absorption of light energy plays a very important role in the determination of photocatalytic activity of any catalyst. The energy required for the transportation of an electron from the valance band to the conduction band is determined by the energy band gap; therefore the UV-DRS result positively predicts the photocatalytic activity of the catalyst. Fig. 6 shows the diffuse reflectance spectra of all the prepared catalysts. Where, Dy_2O_3 has the maximum absorbance in the far UV region, when the doping concentration of ZnO on Dy_2O_3 increases, a shift in absorbance is observed from UV to the visible region. An absorption band around 780–800 nm (shown in the inset of Fig. 6) is observed for all the samples containing Dy_2O_3 and this is due to the characteristic of f–f transition present in lanthanides. ZnDy 50:50 has absorption band around 400 nm close to ZnO in addition to the f–f transition around 780 nm, therefore it has maximum activity in the visible region. The band gap energy of all the prepared catalysts were calculated by plotting $Ah\nu^2$ vs. $h\nu$ as 4.70, 4.67, 3.12, 3.12, 3.10, and 3.07 eV respectively.

A decrease in band gap energy was observed when the doping concentration of ZnO onto Dy_2O_3 increases (pristine Dy_2O_3 , ZnDy 10:90; ZnDy 20:80; ZnDy 30:70; ZnDy 50:50 and pristine ZnO respectively) as illustrated in Fig. S3.

3.7. Analysis of OH radical formation by electron paramagnetic resonance spectroscopy

The visible light photocatalytic activity of the prepared catalyst was tested for the degradation of ORG dye. The mechanism behind the degradation of organics via photocatalytic action would be initiated by the attack of OH radicals formed during the course of the reaction under visible light irradiation. In the present study, the in situ generation of OH radicals by the photocatalyst under visible light irradiation was confirmed using electron paramagnetic resonance spectroscopy by the spin trapping technique, employing DMPO (5,5-dimethyl-1-pyrroline-N-oxide) as the spin trapping agent. Since, the photocatalytic reactions were conducted in the aqueous phase the confirmatory test of the OH radicals formation in the in situ process is given below: required amount of water (50 μl) with catalyst (0.005 mg) and DMPO (40 μl) were taken in a glass tube and the system was irradiated under visible light for about 10 min, then it was centrifuged, subsequently the centrifugate diluted with water then the sample was loaded in the EPR flat cell and the spectra was recorded. The results are shown in Fig. 7, it was observed that the spin trapped DMPO-OH radical signals were appeared at G values of 3412.34, 3427.18, 3442.19 and 3457.01.

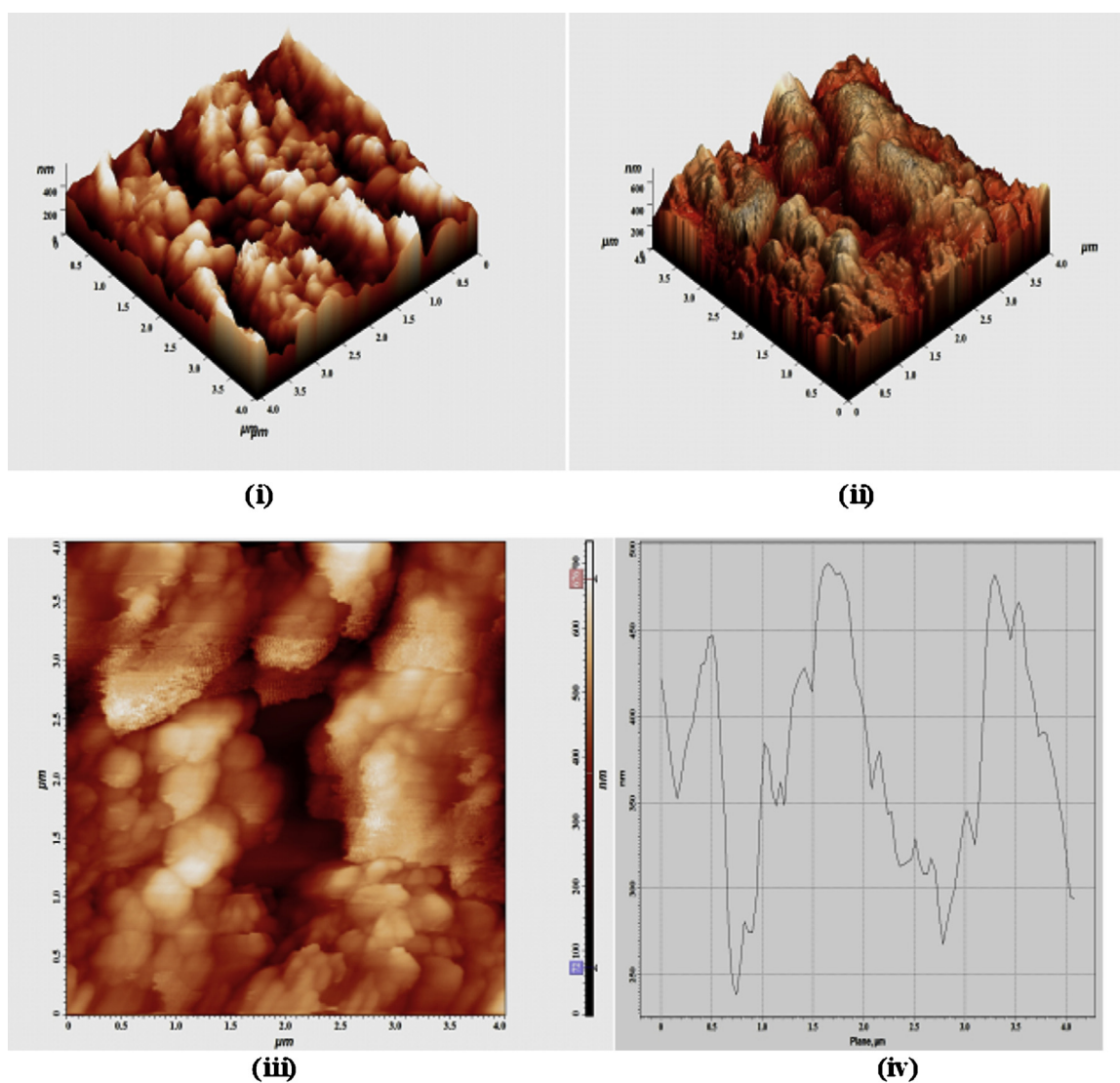


Fig. 5. Atomic force microscopy image of ZnDy 50:50 showing the 3D, 2D images and its surface roughness profile.

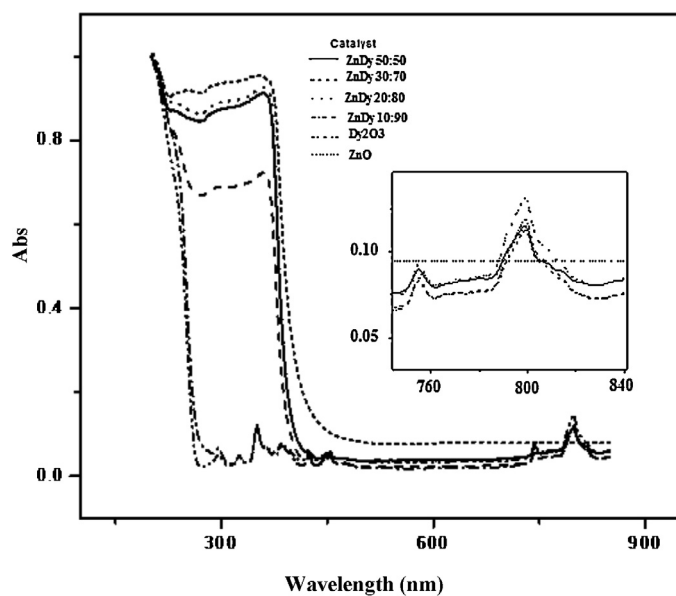


Fig. 6. UV-visible absorption spectra of all the prepared photocatalyst.

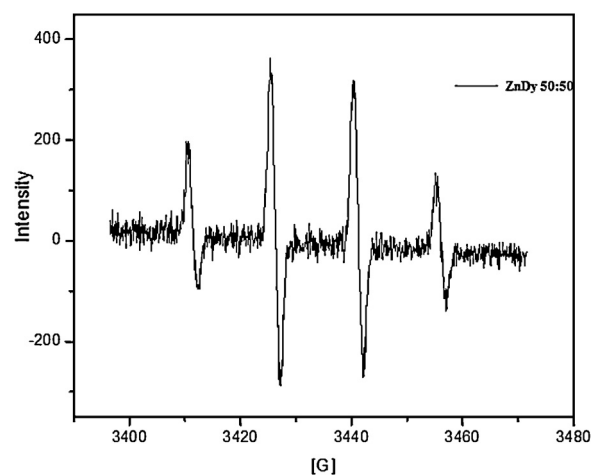


Fig. 7. EPR spectra of the spin trapped OH radical generated in situ by ZnDy 50:50 catalyst via visible light irradiation.

The g factor of free radical was calculated as 2.00782. This confirms that the OH free radicals are generated in the system via the absorption of visible light by the prepared photocatalyst. It also concludes that at the specified concentration of catalyst and reaction time the prepared catalyst ZnDy 50:50 shows that the production of OH radicals, but pristine ZnO and Dy₂O₃ did not produce OH radicals within 10 min of visible light irradiation. Hence, the prepared catalyst is capable of producing OH radicals within a short duration of visible light irradiation and it leads to an enhanced photocatalytic activity for the degradation of ORG dye molecules (discussed latter) when compared to the pristine oxides (Fig. S4).

3.8. Photocatalytic activity of ZnO doped Dy₂O₃

The prepared photocatalyst was found to possess better visible photocatalytic activity based on the analytical observations. From the DRS studies it was observed that on addition of ZnO into the Dy₂O₃ matrix the absorption region of the photocatalyst shifts from the UV region to the visible region. The dysprosium is a rare earth metal belongs to lanthanide group and the element possessing f shells; these f shells are capable of trapping the electrons generated due to visible light absorption by the photocatalyst [68]. As shown in Fig. 6 (inset), the absorbance around 700–800 nm due to the presence of f – f transition. Though the absorption of ZnO is lesser and nearer to the visible region, the photocatalytic activity is not as high when compared to ZnDy 50:50 catalysts and this is due to the recombination of electron-hole pair [69,70]. As the band gap energy is lesser, stability of the excited electron is also very less. But, in the case of the prepared ZnDy 50:50 photocatalyst the band gap energy is comparatively higher than that of pristine ZnO and the excited electron gets trapped by the f shells. Normally, lanthanides have the capability of emitting luminescence [52] which is due to the retardation of light emission. But in the case of ZnDy 50:50 photocatalyst it was observed that before the trapped electron comes to ground state h^+ reacts with the H₂O molecule for the formation of OH free radicals thereby initiating the degradation process. AFM studies also prove that the surface of the synthesized photocatalyst is very rough and porous in nature and this may assist the trapping of the electrons generated during photo process and subsequently absorbs the organic molecules on the surface of the catalyst. The schematic representation of the photocatalytic mechanism is shown in Fig. 8. From EPR results it is concluded that the mechanism of dye degradation is not due to dye sensitization process as the OH radicals are produced in the photo process due to catalytic action even before the addition of dye and also the production of OH radicals is very spontaneous. Therefore dye sensitization if perchance exist is very minimal as the abundance of OH radicals in the system initiates the dye degradation process before getting sensitized.

3.9. Photocatalytic degradation of a model pollutant

3.9.1. Effect of aqueous phase pH on photocatalytic activity

Aqueous phase pH of dye solution greatly influences the degradation efficiency of the organic moiety under visible light irradiation. The pH of the aqueous phase was varied between 2 and 12 by the addition of required amounts of equimolar HCl and NaOH before irradiation. If a particular catalyst is capable of exhibiting photocatalytic activity in a wide range of pH it may be a major benefit in the industrial wastewater treatment as they are not always present at a particular pH. The degradation efficiency of the prepared catalysts are shown in Fig. 9(i) which explains that the catalyst is very active in a wide range of pH and can be effectively used in the industrial wastewater purification processes. The maximum activity is shown by ZnDy 50:50 photocatalyst with 83.85% degradation in neutral pH range when compared to 17.13, 6.91,

Visible Light irradiation

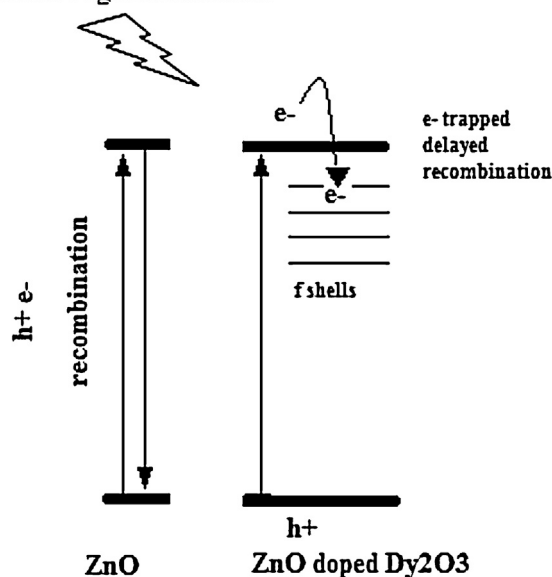


Fig. 8. Mechanism of the photocatalyst under visible light irradiation.

34.89, 48.88 and 41.35% for Dy₂O₃, ZnDy 10:90, ZnDy 20:80, ZnDy 30:70 and ZnO photocatalysts respectively. The reason for lesser activity in acidic and basic pH might be due to the presence of a large amount of H⁺ and OH[−] ions in solution, which competes with the organic moiety for the absorption on the catalyst surface. Also the presence of H⁺ may scavenge the formation of OH radicals thereby suppressing the catalytic activities. Therefore, there is an increase in the percentage of degradation from acidic to neutral pH and then there is a decrease till pH 11. The maximum activity is shown in neutral pH; hence this was used throughout the course of study. And it is shown that the percentage degradation of ZnDy 50:50 photocatalyst is very high compared to that of pristine ZnO.

3.9.2. Variation of catalyst dosage

The dosage of photocatalyst is one of the deciding factors in the examination of degradation efficiency of the target molecules. The effect of catalyst dosage on degradation of ORG was studied with varied catalytic amount from 3 to 20 mg/10 ml for a dye concentration of 5 mg/L and the results are shown in Fig. 9(ii). It was found that at a minimum of 10 mg of catalyst the degradation efficiency was optimum and further addition of catalyst into the system did not enhance the efficiency of dye degradation. The degradation efficiency of all the prepared catalysts are 17.17, 6.91, 34.89, 52.64, 82.78 and 41.35% respectively (Dy₂O₃, ZnDy 10:90, ZnDy 20:80, ZnDy 30:70 and ZnO). The photocatalytic activity of ZnDy 50:50 photocatalyst was nearly double (82.78%) when compared to pristine ZnO (41.35%) under similar conditions. The photocatalytic activity with respect to dopant concentration decreases up to 10 mol% of ZnO doped onto Dy₂O₃ then increases from 20 mol% and exceeds that of pristine ZnO above a particular dopant concentration of 30 mol%. But the results of ZnDy 30:70 are nearly same as the photocatalytic activity of pristine ZnO, therefore ZnDy 50:50 photocatalyst was chosen to be the better proportion among all the prepared catalysts.

3.9.3. Variation of initial dye concentration

The effect of initial dye concentration on photodegradation of ORG dye molecules were studied from 5 to 50 ppm at fixed amount of the catalyst with neutral aqueous phase pH. The results were shown in Fig. 9(iii). It is observed that as the concentration of dye increases there is a decrease in the photocatalytic activity of

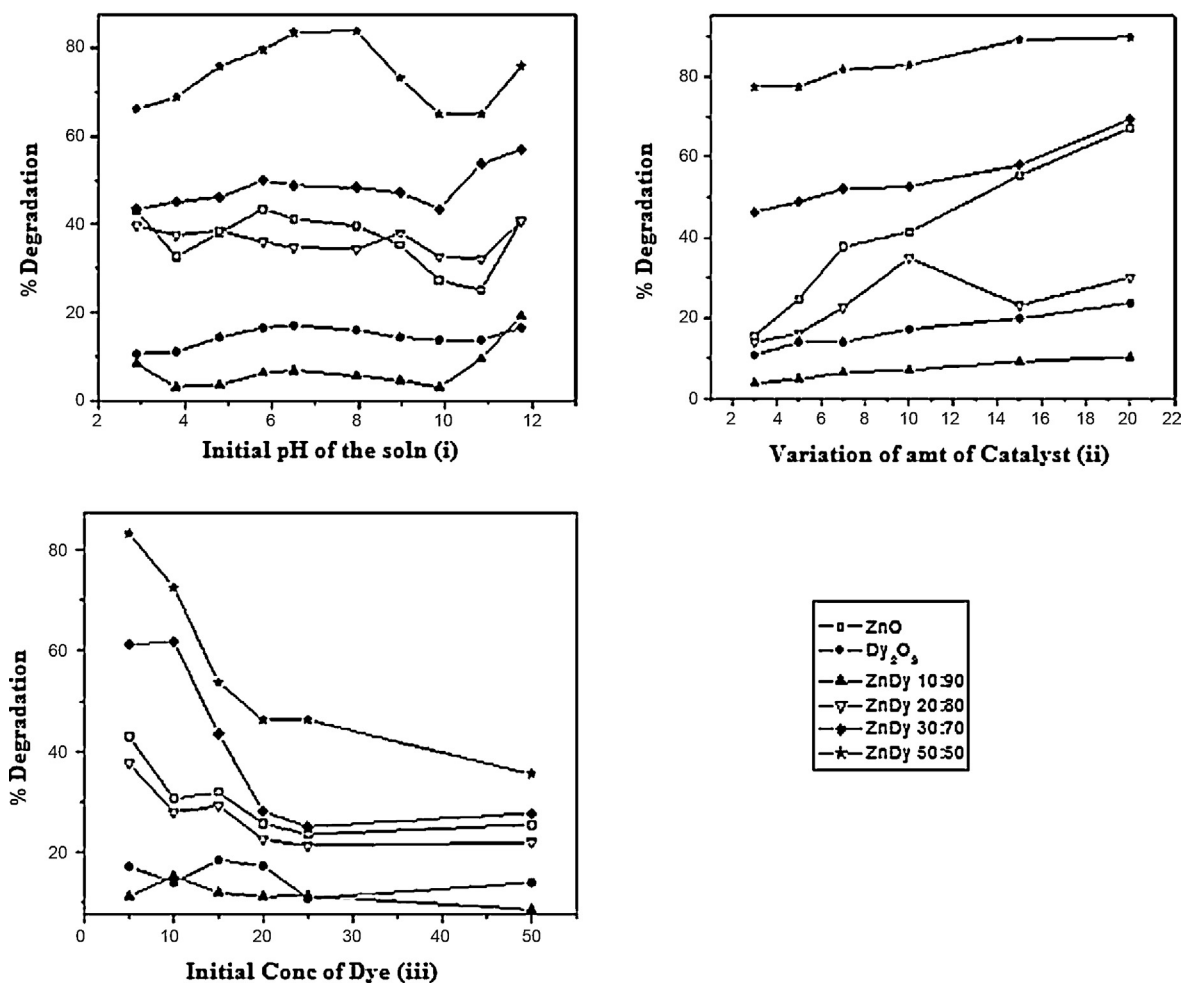


Fig. 9. (i) Effect of initial pH, (ii) variation of catalyst dosage and (iii) variation of initial dye concentration for all the prepared photocatalysts.

the prepared catalyst. For the photocatalyst ZnDy 50:50, the percentage of degradation varied from 83.31% to 35.43% for 5 ppm to 50 ppm respectively and these similar results were also observed for all the prepared photocatalysts. In general as the concentration of dye increased, the percentage degradation decreased. In all the prepared photocatalysts ZnDy 50:50 showed an enhanced photocatalytic activity under present experimental conditions.

3.9.4. Kinetics of visible photocatalytic degradation of ORG

The kinetics of photodegradation was studied with various initial concentrations of ORG dye in visible light irradiation with standard experimental conditions. The preliminary results proved that ZnDy 50:50 photocatalyst possessed a better photoactivity compared to other compositions. So, the kinetics of photodegradation of ORG dye was carried out using ZnDy 50:50 photocatalyst for different initial concentrations which varied from 5 to 25 mg/L. As shown in Fig. 10 the dye molecules were almost completely degraded with ZnDy 50:50 photocatalyst for all the initial concentrations of the dye molecules and these observations were corroborated with reduction in COD level before and after the dye photodegradation. It was observed that for 5 and 10 ppm samples, the COD reduces to nearly zero. For 20 ppm there is a reduction from 600 mg/L to below 100 mg/L and for 25 ppm it reduces from 980 mg/L to less than 200 mg/L, these results suggest that at lower dye concentration, the dye is completely degraded. In general, as the percentage degradation increases the COD of the photodegraded solution decreases which also supports the good

photocatalytic activity of the ZnDy 50:50 under visible light irradiation. The kinetic data were also analyzed in detail and results are shown in Fig. S5. It was noted that the photocatalytic dye degradation process of the ZnDy 50:50 photocatalyst followed a pseudo-first-order kinetics with respect to the initial concentration of the dye $(3) \ln \frac{C_0}{C_e} = k_{obs} \cdot t$ where, C_0 and C_e are the initial and

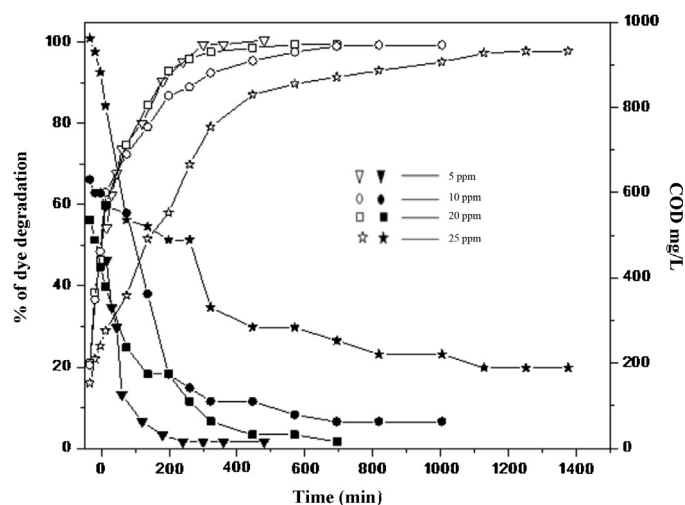


Fig. 10. Comparison of photocatalytic dye degradation and COD of 5, 10, 20 and 25 ppm dye samples for ZnDy 50:50 photocatalyst.

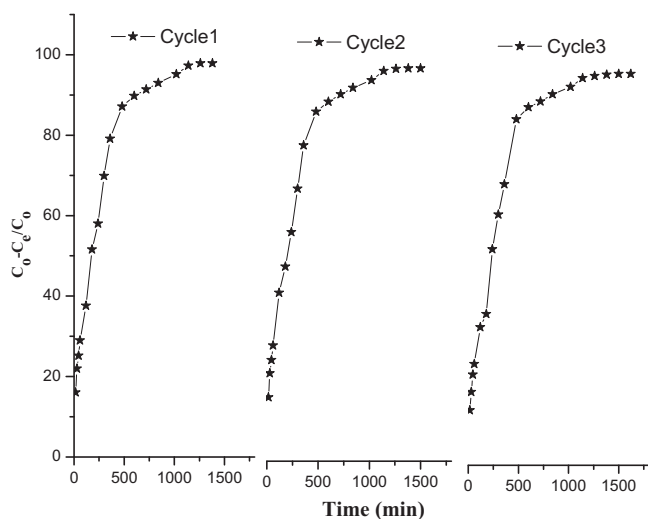


Fig. 11. Reusability studies of the photocatalyst ZnDy 50:50 for 3 cycles.

final concentration of the dye molecules with respective to reaction time “*t*”. The rate constant (k_{obs}) of the reaction varied from 3.33 to $26.32 \times 10^{-3} \text{ min}^{-1}$ and R^2 from 0.987 to 0.994 respectively. The rate constants of the photocatalytic systems were inversely proportional to the initial dye concentrations.

3.9.5. Reusability of the photocatalyst

The reusability of the catalyst is an economic factor, as the cost of the catalyst would be drastically reduced if the numbers of effective cycles were increased without affecting its performance. To test the reusability of ZnDy 50:50 which is considered to be an efficient catalyst, the catalytic activity was checked for three cycles. The results are shown in Fig. 11. It was observed that the catalyst was very active even in the third cycle of operation. The reused ZnDy 50:50 photocatalyst was characterized by FT-IR to check the residues of the target compound and reactive intermediates if they are present in the catalyst. The results are displayed in Fig. S6 and it clearly shows that there is no residues present in the reused catalyst and resemble the original ZnDy 50:50 photocatalyst.

3.9.6. Analysis of by-products by UV-visible spectroscopy

UV-visible absorption spectrum would generally provide valuable information on the probable reaction intermediates and by-products if they were formed during the course of reaction. The absorption peak characteristic of ORG gradually decreased and was nearly zero at 600 min. The absorption spectrum for the kinetics of 10 ppm sample did not show any absorption in the scan range of 200–800 nm, which proves that ORG dye has been degraded completely, without leaving any by-products in the UV-visible region (Fig. S7).

3.9.7. Characterization of by-products formation by QTOF-mass spectroscopy

Neat ORG dye and by-products of photodegraded samples were analyzed by QTOF-mass spectrometry. The mass spectrums of the samples are shown in Figs. S8 and S9. It was observed that the mass spectrum of the original dye sample ORG showed the molecular ion peak at m/e 453 and at m/e 409 which corresponds to the cleavage of two sodium ions. The mass spectra of the photodegraded sample showed a peak at m/e 341 which has the highest molecular weight and it has been further degraded into smaller fragments. These results prove that ORG has been completely degraded and traces are also not present in the degraded aqueous solution.

3.9.8. Mechanism for the photocatalytic degradation of ORG dye

The degradation of the organic molecule was initiated by OH radicals produced by the photocatalyst under visible light irradiation. Initially the OH radicals attack the —N=N— bond in the ORG dye molecule and subsequently the fragmented smaller molecules may undergo further oxidation. Since there is spontaneity in the formation of OH radicals the probability for its attack and further degradation is maximum of the ORG dye molecules. In addition to this, the pH of the photodegraded samples were measured and it was found that there is no change in pH of the aqueous phase after the photocatalytic reaction, these results suggest the absence of acidic or basic by-products.

4. Conclusions

In conclusion, a new visible photocatalyst was developed based on the use of insulator type metal oxides doped by the NC ZnO. In the present study NC ZnO was doped on Dy_2O_3 in various ratios by a simple chemical method and the catalysts prepared were examined for their photocatalytic activity by performing the photodegradation studies by taking ORG as a model pollutant. The NC ZnO doped Dy_2O_3 was characterized by various techniques such as IR, UV-DRS, XRD, FESEM, EDAX, HRTEM, XPS and AFM. The lower band gap (3.1 eV) and the f orbitals present in Dy_2O_3 are responsible for the enhanced visible light photocatalytic activity with a two fold increase compared to pristine ZnO. The characterization of the catalysts clearly confirmed the nano crystallinity and surface roughness. The enhanced visible photocatalytic activity of ZnDy 50:50 is due to the delayed recombination of electron-hole pair, whereas the recombination easily occurs in the case of ZnO. The enhanced visible photocatalytic effect of ZnDy 50:50 may be due to the involvement of f orbitals in retarding the recombination of electron-hole pair and transfer of energy in the photo process which leads to enhanced production of OH radicals and subsequently used in degradation of the ORG dye molecules. The formations of OH radicals were also confirmed by EPR study. The enhanced visible photocatalytic activity of the ZnDy 50:50 photocatalyst was thoroughly tested by the degradation of ORG dye molecules and it was confirmed by UV-visible spectroscopy, COD and QTOF-mass analysis of the photodegraded aqueous phase samples. This study paves way for further studies on insulator metal oxides as one of the major source of oxides for photocatalysis to replace the conventionally used photocatalysts with improved properties.

Acknowledgements

Authors would like thank DST, New Delhi, India for providing a fellowship under INSPIRE and facility provided by INDUSMAGIC 12 FYP program to carried out this work. The authors would like to thank Mrs. J. Sridevi for the analysis of OH radicals by EPR technique.

Appendix A. Supplementary data

Supplementary data associated with this article can be found, in the online version, at <http://dx.doi.org/10.1016/j.apcatb.2013.11.004>.

References

- [1] J.M. Herrmann, *Catal. Today* 53 (1999) 115.
- [2] K. Nakano, E. Obuchi, S. Takagi, R. Yamamoto, T. Tanizaki, M. Taketomi, M. Eguchi, K. Ichida, M. Suzuki, A. Hashimoto, *Sep. Purif. Technol.* 34 (2004) 67.
- [3] P.C. Maness, S. Smolinski, D.M. Blake, Z. Huang, E.J. Wolfrum, W.A. Jacoby, *Appl. Environ. Microbiol.* 65 (1999) 4094.
- [4] A. Fujishima, K. Honda, *Nature* 37 (1972) 238.
- [5] M. Styliadi, D.I. Kondarides, X.E. Verykios, *Appl. Catal. B* 47 (2004) 189.

- [6] T. Bak, J. Nowotny, M. Rekas, C.C. Sorrell, *Int. J. Hydrogen Energy* 27 (2002) 991–1022.
- [7] D. Li, H. Haneda, N.K. Labhsetwar, S. Hishita, N. Ohashi, *Chem. Phys. Lett.* 401 (2005) 579–584.
- [8] A. Fujishima, T.N. Rao, D.A. Tryk, *J. Photochem. Photobiol. C* 1 (2000) 1–21.
- [9] A.J. Nozik, R. Memming, *J. Phys. Chem.* 100 (1996) 13061–13078.
- [10] P. Fernandez-Ibanez, J. Blanco, S. Malato, F. De Las Nieves, *J. Water Res.* 37 (2003) 3180–3188.
- [11] Y. Lu, Y. Lin, T. Xie, S. Shi, H. Fan, D. Wang, *Nanoscale* 4 (2012) 6393–6400.
- [12] H. Li, W. Zhang, S. Huang, W. Pan, *Nanoscale* 4 (2012) 801–806.
- [13] S. Cho, J.-W. Jang, J.S. Lee, K.-H. Lee, *Nanoscale* 4 (2012) 2066–2071.
- [14] Y.-G. Lin, Y.-K. Hsu, Y.-C. Chen, L.-C. Chen, S.-Y. Chen, K.-H. Chen, *Nanoscale* 4 (2012) 6515–6519.
- [15] J. Virkutyte, B. Baruwati, S.V. Rajender, *Nanoscale* 2 (2010) 1109–1111.
- [16] B. Cai, X. Lv, S. Gan, M. Zhou, W. Ma, T. Wu, F. Li, D. Han, L. Niu, *Nanoscale* 5 (2013) 1910–1916.
- [17] Y. Wen, H. Ding, S. Shan, *Nanoscale* 3 (2011) 4411–4417.
- [18] S. Sakthivel, B. Neppolian, M.V. Shankar, B. Arabindoo, M. Palanichamy, V. Murugesan, *Sol. Energy Mater. Sol. Cells* 77 (2003) 65–82.
- [19] I. Nakamura, N. Negishi, S. Kutsuna, T. Ihara, S. Sugihara, K. Takeuchi, *J. Mol. Catal. A: Chem.* 161 (2000) 205–212.
- [20] T. Ihara, M. Miyoshi, Y. Iriyama, O. Matsumoto, S. Sugihara, *Appl. Catal. B: Environ.* 42 (2003) 403–409.
- [21] I. Justicia, G. Garcia, G.A. Battiston, R. Gerbasí, F. Ager, M. Guerra, J. Caixach, J.A. Pardo, J. Riverad, A. Figueras, *Electrochim. Acta* 50 (2005) 4605–4608.
- [22] L. Jianhua, Y. Rong, L. Songmei, *Rare Met.* 25 (2006) 636–642.
- [23] R. Qiu, D. Zhang, Y. Mo, L. Song, E. Brewer, X. Huang, Y. Xiong, *J. Hazard. Mater.* 156 (2008) 80–85.
- [24] L. Song, R. Qiu, Y. Mo, D. Zhang, H. Wei, Y. Xiong, *Catal. Commun.* 8 (2007) 429–433.
- [25] H. Yamashita, M. Harada, J. Misaka, M. Takeuchi, K. Ikeue, M. Anpo, *J. Photochem. Photobiol. A: Chem.* 148 (2002) 257–261.
- [26] Z. Ambrus, N. Balazs, T. Alapi, G. Wittmann, P. Sipos, A. Dombi, K. Mogyorosi, *Appl. Catal. B: Environ.* 81 (2008) 27–37.
- [27] T.A. Egerton, J.A. Mattinson, *J. Photochem. Photobiol. A: Chem.* 194 (2008) 283–289.
- [28] K.G. Kanade, B.B. Kale, J.O. Baeg, S.M. Lee, C.W. Lee, S.J. Moon, H. Chang, *Mater. Chem. Phys.* 102 (2007) 98–104.
- [29] V.R. Shinde, T.P. Gujar, C.D. Lokhande, R.S. Mane, S.H. Han, *Mater. Chem. Phys.* 96 (2006) 326–330.
- [30] G. Wu, A. Chen, *J. Photochem. Photobiol. A: Chem.* 195 (2008) 47–53.
- [31] L. Mingce, C. Weimin, C. Heng, X. Jun, *Front. Chem. China* 2 (2007) 278–282.
- [32] D. Li, H. Haneda, *J. Photochem. Photobiol. A: Chem.* 160 (2003) 203–212.
- [33] H.F. Lin, S.C. Liao, S.W. Hung, *J. Photochem. Photobiol. A: Chem.* 174 (2005) 82–87.
- [34] A.W. Xu, Y. Gao, H.Q. Liu, *J. Catal.* 207 (2002) 151.
- [35] J. Liqiang, S. Xiaojun, X. Baifu, W. Baiqi, C. Weimin, F. Honggang, *J. Solid State Chem.* 177 (2004) 3375.
- [36] K.T. Ranjit, I. Willner, S.H. Bossmann, A.M. Braun, *Environ. Sci. Technol.* 35 (2001) 1544.
- [37] Y. Zhou, S.X. Lu, W.G. Xu, *Environ. Prog. Sustainable Energy* 28 (2009) 226–233.
- [38] S. Anandan, M. Miyauchi, *Phys. Chem. Chem. Phys.* 13 (2011) 14937–14945.
- [39] L. Yang, Y.H. Tang, A.P. Hu, L.D. Zhang, *Phys. B* 403 (2008) 2230.
- [40] S. Shirata, R. Sasaki, T. Kataoka, *Appl. Phys. Lett.* 85 (2004) 2247.
- [41] G.S. Wu, Y.L. Zhuang, Z.Q. Lin, X.Y. Yuan, T. Xie, L.D. Zhang, *Phys. E* 31 (2006) 5.
- [42] R.M. Mohamed, E.S. Aazam, *Desalin. Water Treat.* 50 (2012) 1–7.
- [43] W.H. Strehlow, E.L. Cook, *J. Phys. Chem. Ref. Data* 2 (1973) 163.
- [44] S. Ohmi, C. Kobayashi, I. Kashiwagi, C. Ohshima, H. Ishiura, H. Iwai, *J. Electrochem. Soc.* 150 (2003) 134.
- [45] R.S. Ajimsha, A.K. Das, B.N. Singh, P. Misra, L.M. Kukreja, *Phys. E* 42 (2010) 1838–1843.
- [46] Y.H. Yang, H.G. Zhu, G.W. Yang, *Appl. Phys. A* 103 (2011) 73–79.
- [47] A. Bandyopadhyay, S. Modak, S. Acharya, A.K. Deb, P.K. Chakrabarti, *Solid State Sci.* 12 (2010) 448–454.
- [48] Y. Liu, R. Li, W. Luo, A. Zhu, X. Chen, *Spectrosc. Lett.* 43 (2010) 343–349.
- [49] N. Pandey, R.K. Srivastava, S.G. Prakash, *Indian J. Pure Appl. Phys.* 50 (2012) 260–264.
- [50] A. Joseph, G.L. Praveen, K. Abha, G.M. Lekha, S. George, *J. Lumin.* 132 (2012) 1999–2004.
- [51] H. Huang, Y. Ou, S. Xu, G. Fang, M. Li, X.Z. Zhao, *Appl. Surf. Sci.* 254 (2008) 2013–2016.
- [52] B. Karthikeyan, C.S. Suchand Sandeep, T. Pandiyarajan, P. Venkatesan, Reji Philip, *Appl. Phys. A* 102 (2011) 115–120.
- [53] C. Zhang, Z. Jiang, Z. Wu, J. Chen, P. Yan, J. Wang, *Adv. Mater. Res.* 97–101 (2010) 11–14.
- [54] G.S. Wu, Y.L. Zhuang, Z.Q. Lin, X.Y. Yuan, T. Xie, L.D. Zhang, *Phys. E* 31 (2006) 5–8.
- [55] S. Ji, L. Yin, G. Liu, L. Zhang, C. Ye, *J. Phys. Chem. C* 113 (2009) 16439–16444.
- [56] Z. Li, H. Xue, X. Wang, X. Fu, *J. Mol. Catal. A: Chem.* 260 (2006) 56.
- [57] S. Rengaraj, S. Venkataraj, J.-W. Yeon, Y. Kim, X.Z. Li, G.K.H. Pang, *Appl. Catal. B: Environ.* 77 (2007) 157.
- [58] A. Scalfani, J.M. Hermann, *J. Photochem. Photobiol. A* 113 (1998) 181.
- [59] H. Yang, K. Zhang, R. Shi, A. Tang, *J. Am. Ceram. Soc.* 90 (2007) 1370.
- [60] H.Q. Jiang, P. Wang, X.L. Guo, H.Z. Xian, *Rus. Chem. Bull.* 55 (2006) 1743.
- [61] A.S. Weber, A.M. Grady, R.T. Koodali, *Catal. Sci. Technol.* 2 (2012) 683–693.
- [62] R.Y. Hong, J.H. Li, L.L. Chen, D.Q. Liu, H.Z. Li, Y. Zheng, J. Ding, *Powder Technol.* 189 (2009) 426–432.
- [63] Y. Zhang, K.L. Zhang, M.K. Jia, H. Tang, J.T. Sun, L.J. Yuan, *Chin. Chem. Lett.* 13 (2002) 587–589.
- [64] S. Menon, B. Dhabeekar, E. Alagu Raja, S.P. More, T.K. Gundu Rao, R.K. Kher, *J. Lumin.* 128 (2008) 1673.
- [65] K.K. Satapathy, F. Khan, *Adv. Mater. Lett.* 4 (2013) 323–326.
- [66] R. John, R. Rajakumari, *Nano Micro Lett.* 4 (2012) 65–72.
- [67] R. Elilarrasi, G. Chandrasekaran, *Am. J. Mater. Sci.* 2 (2012) 46–50.
- [68] T. De Zhao, J. Peng, C. Xiao, X. Yan, Ke, *Mater. Lett.* 61 (2007) 105.
- [69] C.Q. Chen, Y.H. Zheng, Y.Y. Zhan, X.Y. Lin, Q. Zheng, K.M. Wei, *Dalton Trans.* 40 (2011) 9566–9570.
- [70] J.G. Yu, X.X. Yu, *Environ. Sci. Technol.* 42 (2008) 4902–4907.